



Passive ankle and hindfoot kinematics within a robot-driven tibial movement envelope

Anthony H. Le^a , Andrew C. Peterson^b, Jordy A. Larrea Rodríguez^c, Takuma Miyamoto^{d,e}, Florian Nickisch^e, Amy L. Lenz^{b,*}

^a Department of Biomedical Engineering, University of Utah, 36 S Wasatch Drive, Salt Lake City, UT 84112, USA

^b Department of Mechanical Engineering, University of Utah, 1495 E 100 S, Salt Lake City, UT 84112, USA

^c Department of Electrical and Computer Engineering, University of Utah, 50 S Central Campus Dr, Salt Lake City, UT 84112, USA

^d Department of Orthopaedic Surgery, Nara Medical University, 840 Shijo, Kashihara, Nara 6348521, Japan

^e Department of Orthopaedics, University of Utah, 590 Wakara Way, Salt Lake City, UT 84108, USA

ARTICLE INFO

Keywords:

Foot and ankle
Passive kinematics
Robotics
Cadaveric simulations
Underfoot perturbations

ABSTRACT

Accurate description of individual bone kinematics is essential for understanding individual foot and ankle joint function and interactions. While invasive and noninvasive techniques, including robotic simulators, have advanced the direct measurement of individual joint kinematics during gait, efforts to quantify the passive adaptability of the foot and ankle remain limited. This study aimed to systematically describe the passive kinematics and ranges of motion of the ankle and hindfoot joints during prescribed planar tibial motions. Five fresh-frozen lower limb cadaveric specimens were attached to a 6-axis industrial robot, loaded to 25 % body weight, and prescribed tibial dorsi/plantarflexion, external/internal rotation, and varus/valgus alignment motions with various underfoot perturbations. Tibiotalar, talofibular, tibiofibular, subtalar, talonavicular, and calcaneocuboid joint kinematics were calculated using joint-specific anatomical coordinate systems. One-way repeated measures ANOVA with post hoc Bonferroni corrections ($\alpha = 0.05$) compared joint rotations and range of motions (ROM) across various underfoot perturbations. Significant passive adaptive kinematic changes occurred in the hindfoot joints during prescribed dorsi/plantarflexion and external/internal rotation, indicated by functional shifts in hindfoot kinematics with different perturbations, while ROM remained consistent. In contrast, minimal passive adaptive motions were observed in the hindfoot joints during varus/valgus alignment, indicating a reduced role in foot mobility during coronal plane tibial motion. These findings emphasize the importance of accurately measuring individual bone kinematics, particularly the significant contributions of hindfoot joints to the passive mobility and stability of the foot and ankle.

1. Introduction

The foot and ankle complex is a highly intricate system of articulating joints essential for mobility and stability during lower limb ground interaction. Notably, the foot and ankle can passively conform to uneven or variable surfaces to maintain balance and stability. To understand its passive adaptive functionalities for providing a stable base of support, an accurate description of individual bone kinematics is needed (Whittaker et al., 2011). In turn, we can delineate the individual contributions of each joint and their interactions in the overall mobility and stability of the foot and ankle. Passive motions, in particular, can

reveal the inherent structural characteristics of the joint, including their range of motion (ROM) and alignment. However, obtaining a comprehensive description of passive foot and ankle motions remains a significant challenge.

Recent research has made strides in accurately describing individual bone motions *in vivo*. Invasive methods, such as surgically placed bone pins, have provided comprehensive kinematic data. For example, Arndt et al. found significant mobility in the talonavicular joint and some motion between the tibia and fibula during running using intracortical pins (Arndt et al., 2007), while Lundgren et al. highlighted variability in the talocalcaneal joint and motion in the medial cuneiform-navicular

* Corresponding author at: Department of Mechanical Engineering, University of Utah, 1495 E 100 S, Salt Lake City, UT 84112, USA.

E-mail addresses: anthony.le@utah.edu (A.H. Le), andrew.c.peterson@utah.edu (A.C. Peterson), jordy.larrea@utah.edu (J.A. Larrea Rodríguez), tmiyamoto@naramed-u.ac.jp (T. Miyamoto), florian.nickisch@hsc.utah.edu (F. Nickisch), amy.lenz@utah.edu (A.L. Lenz).

joint during gait (Lundgren et al., 2008). In contrast, noninvasive techniques for capturing individual *in vivo* joint kinematics in the foot and ankle during gait have also been employed, such as biplane fluoroscopy imaging (Bey et al., 2008; Bey et al., 2006; Campbell et al., 2016; Kapron et al., 2014; Roach et al., 2016; Wang et al., 2015), and four-dimensional magnetic resonance imaging and computed tomography (CT) (Miyamoto et al., 2023; Postolka et al., 2024). However, *in vivo* studies are limited by small, heterogeneous populations, high costs, and time-consuming requirements for longitudinal protocols, often focusing on joint kinematics during gait.

Robotic simulators offer an alternative approach by manipulating cadaveric joints to assess *in vitro* biomechanics reliably and repetitively (Aubin and Ledoux, 2023; Aubin et al., 2008; Aubin et al., 2011; Baxter et al., 2016; Noble et al., 2010; Salb et al., 2016; Whittaker et al., 2011). Particularly, dynamic gait simulators have been used to accurately reproduce physiological gait and describe the kinematics of tarsal and midtarsal bones (Baxter et al., 2016; Nester et al., 2007; Whittaker et al., 2011). Like *in vivo* studies, these *in vitro* studies, while contributing valuable kinematic interpretations of the foot and ankle, have predominately focused on simulating gait in cadavers. Thus, limited efforts have been made to quantify the passive adaptability of the foot and ankle under different loading conditions.

Passive foot kinematics have been studied using sequences of static poses of cadavers in clinical or weightbearing CT (Burssens et al., 2021; Conconi et al., 2024a; Conconi et al., 2024b). However, these methods are limited. They can only provide snapshots of the joint, potentially missing transitional movements between static states. As a result, subtle but important variations in motion patterns, such as those induced by changes in load or surface conditions, may be overlooked. This limitation can lead to an incomplete understanding of the joint's passive behavior throughout its full ROM during ground interactions. Furthermore, these static measurements cannot account for the continuous interplay between different joints and their adaptive responses. Consequently, while these prior methods provide some insight, they fail to capture the full complexity and variability of passive foot and ankle motions.

Therefore, the purpose of the present study was to systematically describe the passive joint kinematics and ROM of the ankle and hindfoot during continuously prescribed planar tibial motions under weight-bearing conditions, incorporating various underfoot perturbations to replicate physiological foot and ankle orientations and simulate forefoot interactions with uneven surfaces (Conconi et al., 2024a; Downey et al., 2022; Tuijthof et al., 2009). We hypothesized that individual ankle and hindfoot joints will passively adapt to underfoot perturbations through kinematic shifts, while the overall range of motion experienced by the joints will remain unchanged. This study builds on weightbearing CT studies and leverages robotic cadaveric simulation, providing new insights into passive joint behavior relative to continuous tibial motion and weightbearing.

2. Materials and methods

2.1. Cadaveric specimen preparation

Five fresh-frozen tibia-to-toe tip cadaveric specimens (5 males; 53 ± 13 yrs old) with no history of foot and ankle injury or surgery were procured under University of Utah Institutional Review Board approval. Conventional fan beam CT scans were acquired using a Siemens SOMATOM Force scanner (120 kVp, 100 mAs, 0.6 mm isotropic) and segmented to generate three-dimensional (3D) reconstructed full-length tibia and fibula bone models in Mimics v24.0 (Mimics Innovation Suite, Materialise). Specimens were dissected approximately 120 mm distal to the tibial plateau, preserving the proximal tibial/fibular interosseous membrane while removing all soft tissues. Specimen-specific molds were 3D-printed from tibia and fibula bone models to encase the proximal tibia in isolation and rigidly affix to a 6-axis industrial robotic

manipulator end-effector (M-20iA, FANUC America) equipped with a 6-axis force sensor (FS-40iA, FANUC America), while allowing free fibular motion and establishing a sensible kinematic relationship between the robotic manipulator and tibia (Fig. 1).

Anatomical local coordinate system (LCS) of the tibia was defined at the tibiotalar joint center using Automatic Anatomical Foot and Ankle Coordinate Toolbox (AAFACT) developed in our lab (Knutson et al., 2024; Lenz et al., 2021; Muhlrud et al., 2024; Peterson et al., 2023) and set as the robot's tool center point (i.e., center of rotation). End-effector force sensor's Z-axis was aligned with the tibia's inferior-to-superior anatomical axis, while its X-axis and Y-axis were aligned with the tibia's medial-to-lateral and posterior-to-anterior axes, respectively.

2.2. Motion capture

Infrared marker clusters were attached to the tibia, fibula, talus, calcaneus, navicular, cuboid, 1st metatarsal (MT1), and 5th metatarsal (MT5) bones via custom radiopaque 3D-printed bone pins through skin portals (Fig. 1). Bone pins were placed under fluoroscopy to ensure that joint spaces were not breached, and manual manipulation confirmed rigid fixation. Rigid body motion of each marker was tracked in 6 degrees of freedom (DOF; 3 translations and 3 rotations) at 250 Hz using an active optical motion capture system (Optotrak Certus, NDI) and described with time-dependent 4 × 4 homogeneous transformation matrices.

2.3. Data Collection

Using tuned specimen-specific tibial motion profiles, each specimen was loaded to 25 ± 2.5 % body weight (BW) in a neutral position at 1 mm/s and robotically prescribed tibial dorsiflexion/plantarflexion (DF/PF), external/internal rotation (ER/IR), and varus/valgus alignment (VR/VG) rotation at 2°/s (2 Hz) to their respective tibial ROM endpoints under 6 underfoot perturbation conditions: (1) flat, (2) 45° toe wedge for metatarsophalangeal (MTP) joint DF, (3) 0.5-in block under MT1, (4) 0.5-in block under MT5, (5) 10° eversion (EV), and (6) 10° inversion (INV) (Fig. 1). Details about the tibial motion profile tuning procedure to determine tibial ROM endpoints can be found in Appendix A of the Supplementary Material. Toe wedges and metatarsal blocks were 3D-printed and positioned under the foot. A custom adjustable platform, capable of rotating and locking in 5° increments, prescribed 10° EV and INV in the coronal plane (Fig. 1).

2.4. Data Processing

Cone beam CT scans were acquired using a Curvebeam PedCAT scanner (120 kVp, 5 mAs, 0.4 mm isotropic) and segmented using Mimics v24.0 (Mimics Innovation Suite, Materialise) to register the individual transformations between marker clusters and bone LCS defined using AAFACT (Peterson et al., 2023). Transformation matrices relating the marker cluster LCS to the bone LCS were calculated using the object registration and transformation matrix functions in 3-Matic v16.0 (Mimics Innovation Suite, Materialise). For each underfoot perturbation, tibiotalar (TT), talofibular (TaF), tibiofibular (TiF), subtalar (ST), talonavicular (TN), and calcaneocuboid (CC) joint rotations were calculated from the transformation matrices via Euler decomposition and Cardan sequences and normalized to initial joint angles measured in the loaded, neutral position on the flat surface (Grood and Suntay, 1983; MacWilliams and Davis, 2013). Joint rotations and ROM were reported relative to the anatomical LCS of the proximal bone of the joint, ensuring consistency with the respective anatomical orientation of each individual joint.

Cardan sequences refer to a specific type of rotation sequence used in calculating joint angles and 3D kinematics and strictly involves rotations about 3 different axes (Grood and Suntay, 1983; MacWilliams and Davis, 2013; Wu et al., 2005). X-axis was defined as the medial-to-lateral

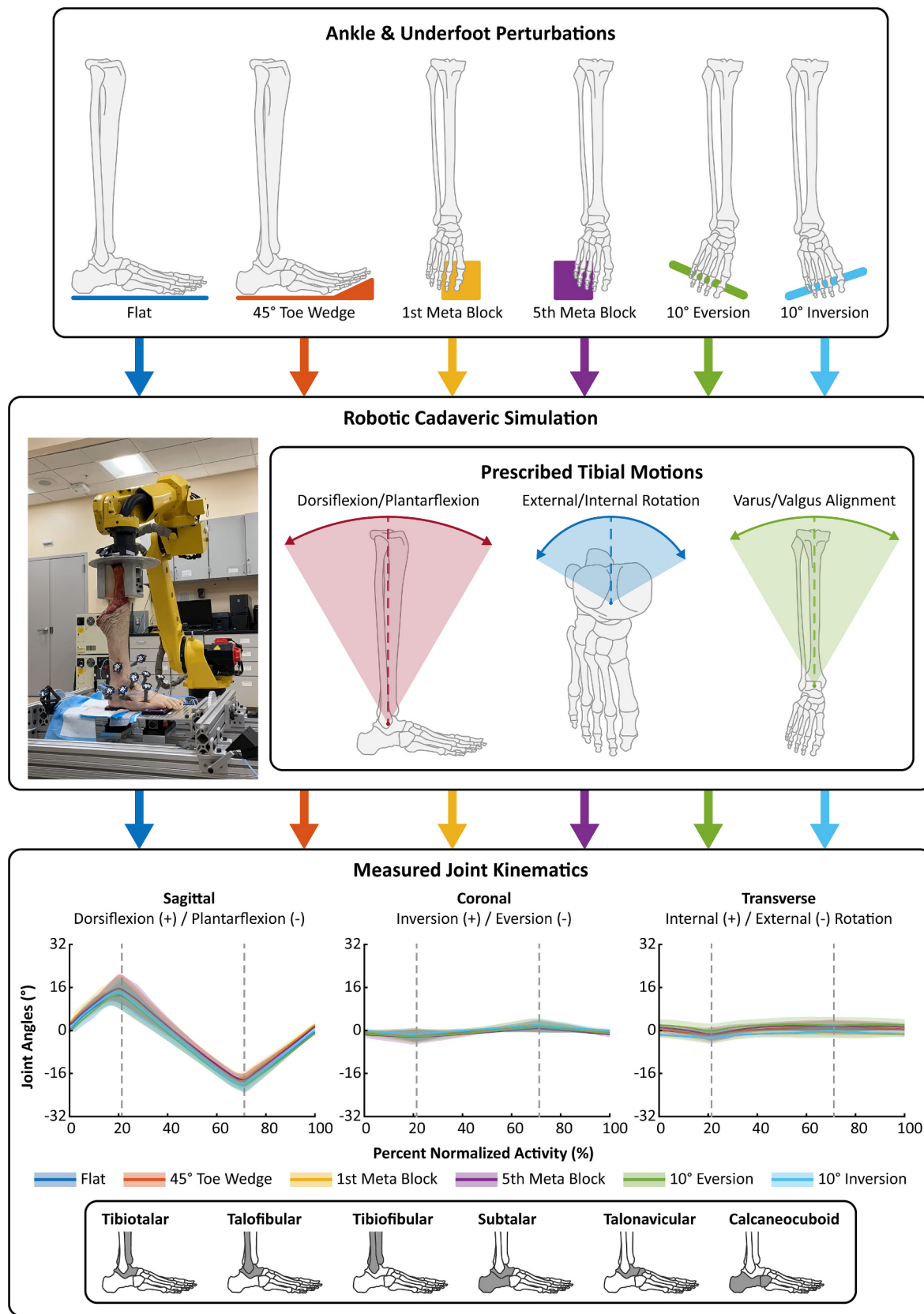


Fig. 1. Robotic cadaveric simulation of passive planar tibial motions with various forefoot and ankle perturbations. Tibiotalar, talofibular, tibiofibular, subtalar, talonavicular, and calcaneocuboid joint angles were measured in the sagittal, transverse and coronal planes during prescribed dorsiflexion/plantarflexion, internal/external rotation, and varus/valgus alignment.

direction, Y-axis as the posterior-to-anterior direction, and Z-axis as the inferior-to-superior direction, consistent with the right-hand rule. TT joint followed the XYZ sequence; TiF, TaF, TN, and CC joints followed the ZYX sequence; and ST joint followed the YXZ sequence.

2.5. Statistical Analyses

One-way repeated measures ANOVA (RMANOVA) temporal statistical parametric mapping (SPM) analysis ($\alpha = 0.05$) was used to compare individual passive joint rotations across perturbations followed by post hoc pairwise comparisons with Bonferroni correction for parametric data or post hoc non-parametric permutation testing for non-parametric data (Nichols and Holmes, 2002) at each instance of normalized percent activity using the MATLAB-based spm1d package (MATLAB R2023a, MathWorks) (Pataky, 2010; Pataky et al., 2013, 2016; Pataky et al., 2015). One-way RMANOVA was also used to compare the mean passive ROM at each joint across all conditions followed by Tukey HSD post hoc pairwise comparisons for parametric ROM data or post hoc pairwise comparisons with Dunn-Sidak Correction for non-parametric ROM data (R 4.3.0, RStudio, Posit). Significance level was set a priori at $\alpha = 0.05$. Normality of joint rotations and ROM was assessed with the Shapiro-Wilk test, and homogeneity of variance with the Levene test. For conciseness, only pairwise comparisons relative to the flat condition, used as the baseline, were reported for observed changes due to perturbations. Minimum detectable difference (MDD) was calculated for each joint ROM to estimate the smallest detectable change across perturbation, accounting for variance, sample size, and statistical power (80 %), and a significance level of $\alpha = 0.05$.

3. Results

3.1. Tibial rotation endpoints

During the tibial motion profile tuning procedure, mean tibial DF and PF rotations from neutral position were $14.2^\circ \pm 1.7^\circ$ and $22.2^\circ \pm 2.6^\circ$, respectively. Mean tibial ER and IR from neutral position were $19.4^\circ \pm 1.0^\circ$ and $17.6^\circ \pm 1.9^\circ$, respectively. Mean tibial VR and VG rotations from neutral position were $10.4^\circ \pm 1.7^\circ$ and $13.4^\circ \pm 1.9^\circ$, respectively.

3.2. Prescribed tibial Dorsiflexion/Plantarflexion (DF/PF) motion

During prescribed tibial DF/PF, TT, TaF, and TiF joints exhibited minimal passive adaptation to underfoot perturbations across all planes (Fig. 2). In contrast, ST and TN joints showed significant passive adaptations in the transverse and coronal planes between peak prescribed DF and PF, while CC joint demonstrated significant adaptations in the sagittal and coronal planes throughout most of the prescribed DF/PF (Fig. 2).

With a 45° toe wedge, ST joint showed increased INV and IR, while TN and CC joints showed increased PF, INV, and IR throughout prescribed DF/PF. Similarly, with a block under MT1 and 10° INV, ST and TN joints showed increased INV and IR, while CC joint showed increased PF and INV between peak prescribed DF and PF. In contrast, with a block under MT5 and 10° EV, TN joints showed instances of increased DF, but both ST and TN joints showed increased EV and ER between peak prescribed DF and PF. CC joint showed increased DF, EV, and ER throughout prescribed DF/PF.

Passive ROM across all joints were not significantly different with any perturbation type compared to no perturbation across all planes during prescribed DF/PF. (Fig. 3). MDD for passive joint ROM ranged from 0.10° to 4.17° across all planes during prescribed DF/PF.

3.3. Prescribed tibial external/internal (ER/IR) motion

During prescribed tibial ER/IR, TT and TaF joints showed some

passive adaptation to underfoot perturbations in the sagittal plane, while ST and TN joints passively adapted in the transverse and coronal planes between peak prescribed ER and IR. CC joint demonstrated significant passive adaptations in the sagittal and coronal planes throughout most of the prescribed ER/IR (Fig. 4).

With a 45° toe wedge and a block under MT1 and MT5, TT and TaF joints showed increased DF and PF, respectively, throughout prescribed ER/IR. With 10° INV, TaF joint also showed increased PF when returning to neutral from peak prescribed IR. With a 45° toe wedge, ST joint showed increased INV and IR, while TN and CC joints showed increased PF, INV, and IR between peak prescribed ER and IR. With a block under MT1 and 10° INV, ST joint showed increased INV and IR, TN joint only showed increased INV, and CC joint showed increased PF and INV between peak prescribed ER and IR. With 10° INV, TN joint showed increased IR between peak prescribed ER and IR. With a block under MT5 and 10° EV, ST and TN joints showed increased EV and ER, while CC joint showed increased EV between peak prescribed ER and IR. With a block under MT5 only, CC showed increased DF through the entire duration of prescribed ER/IR and instances of increased EV and ER.

In the sagittal plane, TaF joint showed decreased passive ROM with a block under MT1 ($3.57^\circ \pm 0.94^\circ$, $p = 0.04$) and 10° INV ($3.35^\circ \pm 0.80^\circ$, $p = 0.008$) compared to no perturbation ($4.60^\circ \pm 1.25^\circ$) (Fig. 5). Otherwise, passive ROM in the other joints were not significantly different with any perturbation type across all planes during prescribed ER/IR. (Fig. 5). MDD for passive joint ROM ranged from 0.21° to 3.88° across all planes during prescribed ER/IR.

3.4. Prescribed tibial varus/valgus alignment (VR/VG) motion

During prescribed tibial VR/VG, TT and TaF joints showed some passive adaptation to the underfoot perturbations in the sagittal plane between peak VR and VG (Fig. 6). ST, TN, and CC joints showed minimal passive adaptation to the underfoot perturbations across all planes primarily at the beginning and/or end of the prescribed VR/VG (Fig. 6).

With a 45° toe wedge, TT and TaF joints showed increased DF and PF, respectively, between peak prescribed VR and VG. With a block under MT1 and MT5, TT and TaF joints showed increased DF and PF, respectively, and IR and ER, respectively, while TaF joint also showed some instances of increased EV between peak prescribed VR and VG. With a 45° toe wedge, TN showed increased PF, INV, and IR, while CC joint showed increased PF and INV between peak prescribed VR and VG. With a block under MT1 and 10° INV, ST and TN joints showed increased INV and IR, while CC joint showed increased PF and INV at the beginning and/or end of prescribed VR/VG motion. With a block under MT5 and 10° EV, ST and TN joints showed increased EV and ER, while CC joint showed increased DF and EV at the beginning and/or end of prescribed VR/VG.

Passive ROM across all joints were not significantly different with any perturbation type compared to no perturbation across all planes during prescribed VR/VG (Fig. 7). MDD for passive joint ROM ranged from 0.13° to 4.31° across all planes during prescribed VR/VG.

4. Discussion

In this study, we systemically described the passive kinematics and ROM of the ankle and hindfoot joints during robotically prescribed tibial DF/PF, ER/IR, and VR/VG. We demonstrated how individual ankle and hindfoot joints passively adapt to various underfoot perturbations compared to no perturbation (i.e., flat), with perturbations chosen to replicate physiological foot orientations and simulate forefoot interactions with uneven surfaces (Conconi et al., 2024a; Downey et al., 2022; Tuijthof et al., 2009).

During prescribed tibial DF/PF, TT, TaF, and TiF joints generally exhibited minimal passive adaptive motions in response to the perturbations. This suggests that the ankle joints, particularly the TT joint, play a more limited role in passively adapting to perturbations, supporting

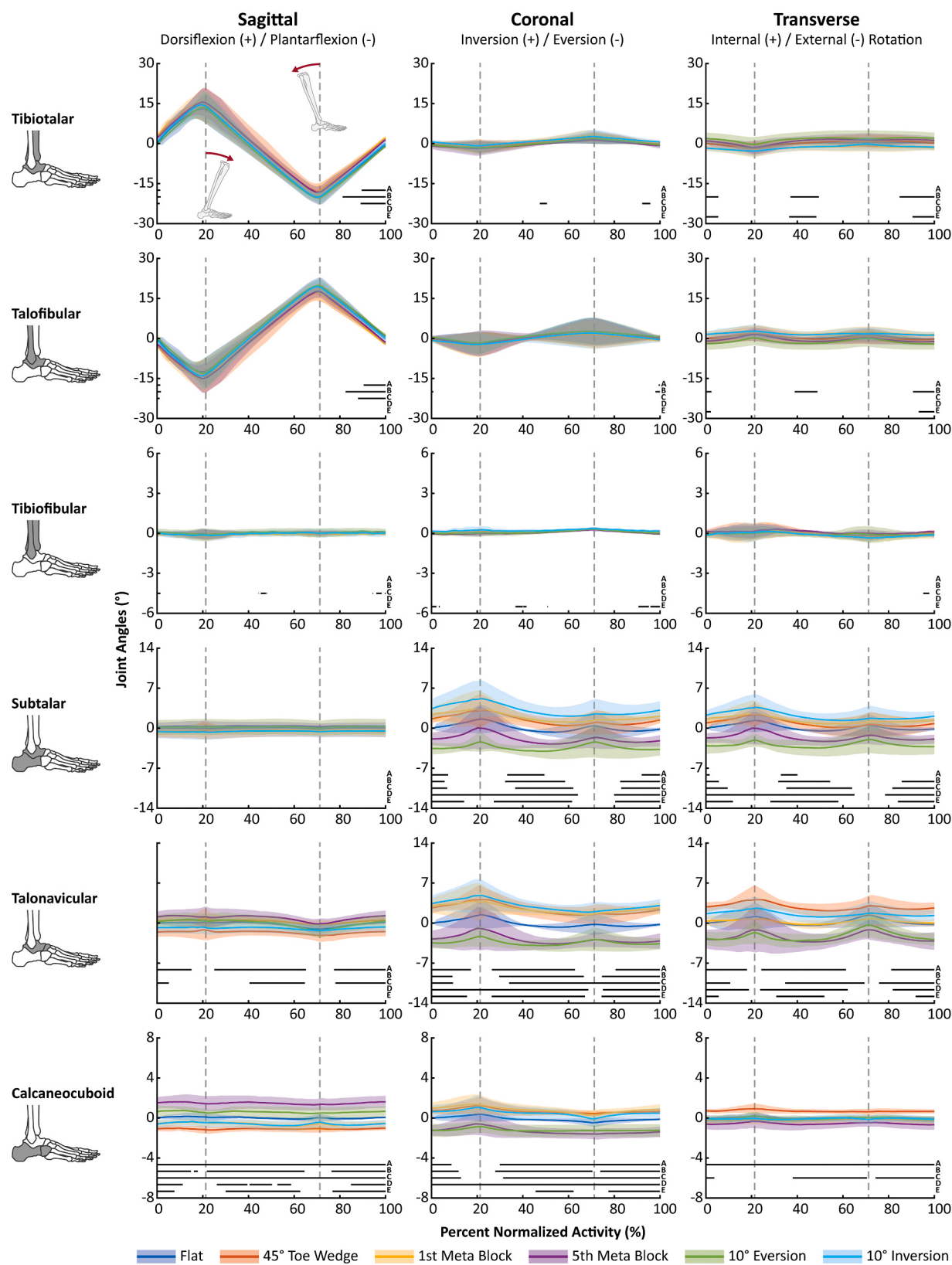


Fig. 2. Mean (\pm SD) tibiotalar, talofibular, tibiofibular, subtalar, talonavicular, and calcaneocuboid joint kinematics in the sagittal, transverse, and coronal plane during prescribed tibial dorsiflexion/plantarflexion motion for each condition. Black horizontal bars indicate portions of prescribed motion where joint kinematics were significantly different between flat versus (A) 45° toe wedge, (B) 0.5-in block under 1st metatarsal, (C) 0.5-in block under 5th metatarsal, (D) 10° eversion, and (E) 10° inversion ($\alpha < 0.05$). First grey vertical dashed line indicates peak prescribed dorsiflexion. Second grey vertical dashed line indicates peak prescribed plantarflexion.

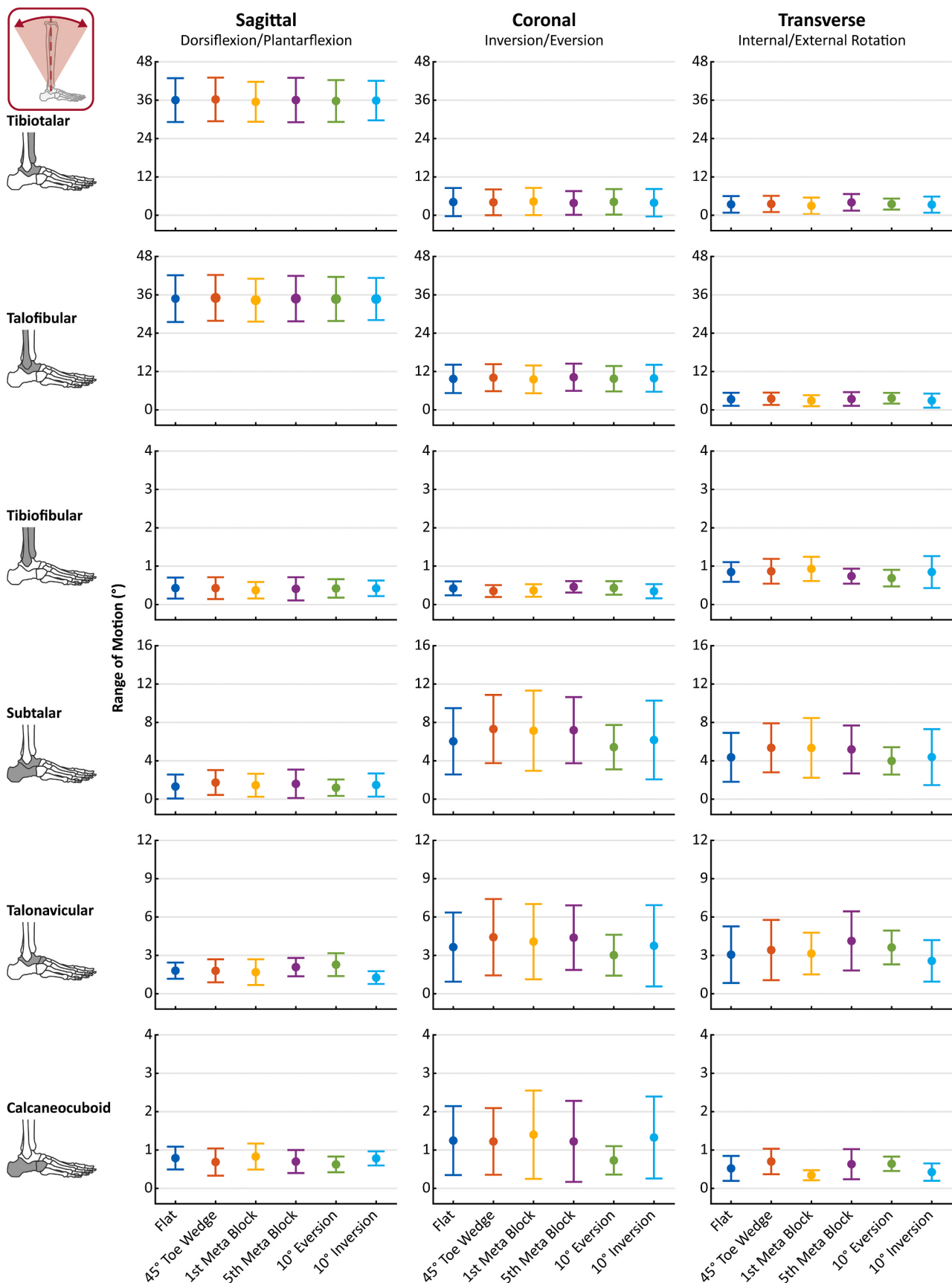


Fig. 3. Mean (\pm SD) tibiotalar, talofibular, tibiofibular, subtalar, talonavicular, and calcaneocuboid joint ROM in the sagittal, transverse, and coronal plane during prescribed tibial dorsiflexion/plantarflexion motion for each condition. Asterisk (*) indicate a significant difference from flat, i.e., no perturbation ($\alpha < 0.05$).

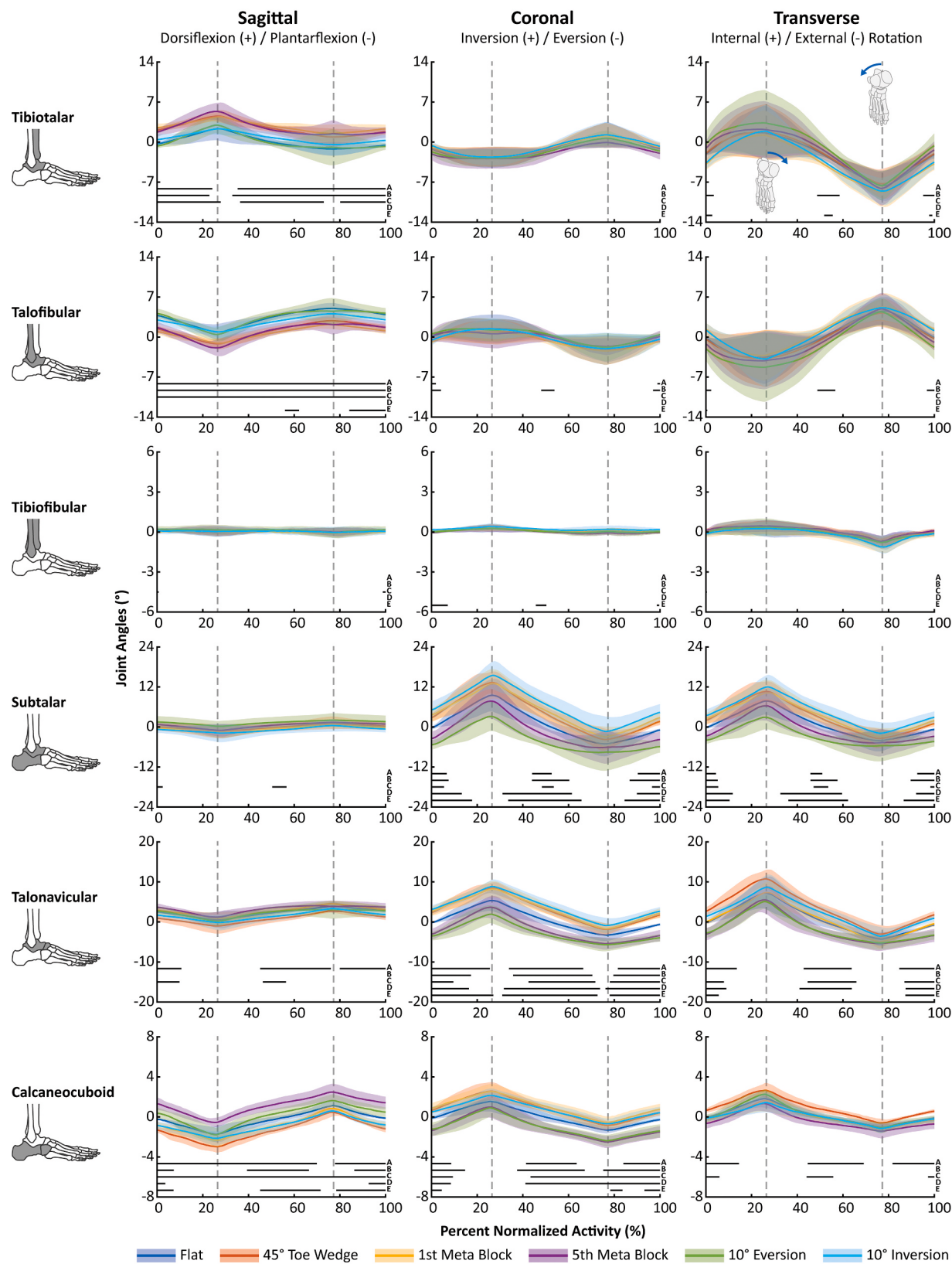


Fig. 4. Mean (\pm SD) tibiotalar, talofibular, tibiofibular, subtalar, talonavicular, and calcaneocuboid joint kinematics in the sagittal, transverse, and coronal plane during prescribed tibial internal/external rotation motion for each condition. Black horizontal bars indicate portions of prescribed motion where joint kinematics were significantly different between flat versus (A) 45° toe wedge, (B) 0.5-in block under 1st metatarsal, (C) 0.5-in block under 5th metatarsal, (D) 10° eversion, and (E) 10° inversion ($\alpha < 0.05$). First grey vertical dashed line indicates peak tibial external rotation Second grey vertical dashed line indicates peak tibial internal rotation.

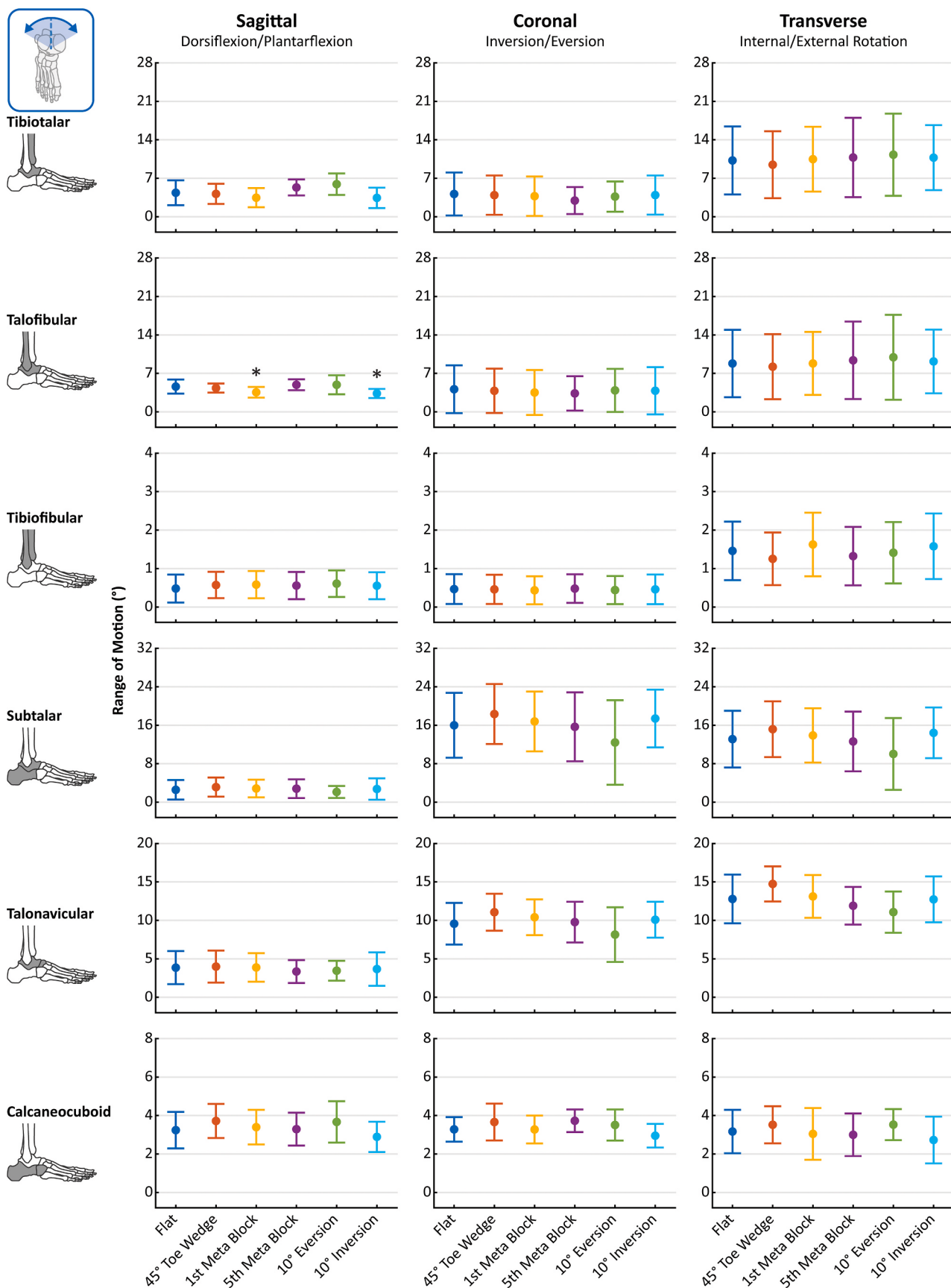


Fig. 5. Mean (\pm SD) tibiotalar, talofibular, tibiofibular, subtalar, talonavicular, and calcaneocuboid joint ROM in the sagittal, transverse, and coronal plane during prescribed tibial internal/external rotation motion for each condition. Asterisk (*) indicate a significant difference from flat, i.e., no perturbation ($\alpha < 0.05$).

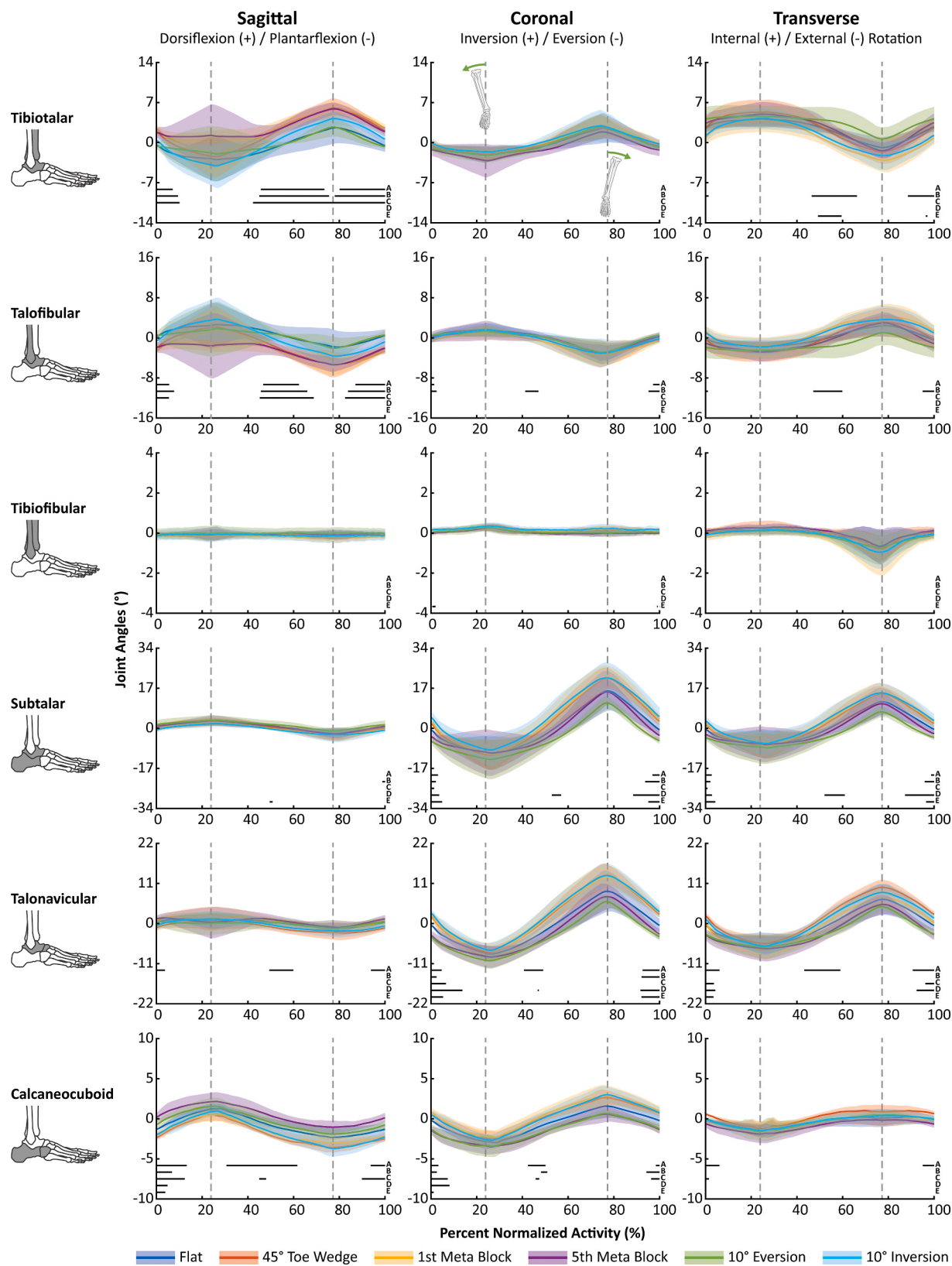


Fig. 6. Mean (\pm SD) tibiotalar, talofibular, tibiofibular, subtalar, talonavicular, and calcaneocuboid joint kinematics in the sagittal, transverse, and coronal plane during prescribed tibial varus/valgus alignment motion for each condition. Black horizontal bars indicate portions of prescribed motion where joint kinematics were significantly different between flat versus (A) 45° toe wedge, (B) 0.5-in block under 1st metatarsal, (C) 0.5-in block under 5th metatarsal, (D) 10° eversion, and (E) 10° inversion ($\alpha < 0.05$). First grey vertical dashed line indicates peak prescribed varus alignment. Second grey vertical dashed line indicates peak prescribed valgus alignment.

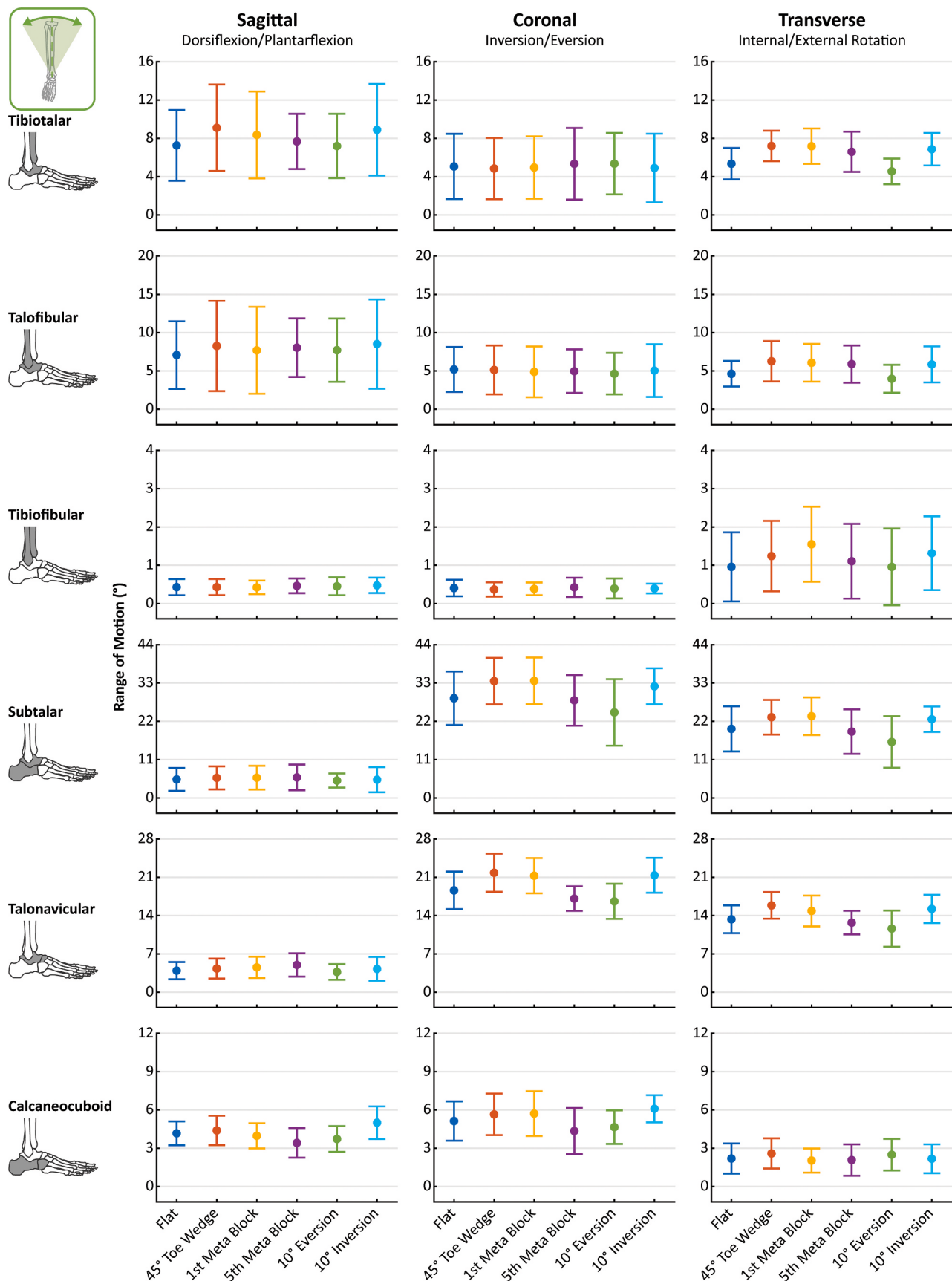


Fig. 7. Mean (\pm SD) tibiotalar, talofibular, tibiofibular, subtalar, talonavicular, and calcaneocuboid joint ROM in the sagittal, transverse, and coronal plane during prescribed tibial varus/valgus alignment motion for each condition. Asterisk (*) indicate a significant difference from flat, i.e., no perturbation ($\alpha < 0.05$).

recent findings that challenge the traditional view of the TT joint as a primary contributor to foot and ankle mobility (Lundgren et al., 2008; Whittaker et al., 2011). However, notable passive adaptive motions of the talus were observed. First, TT and TaF joints showed increased DF when returning to neutral from peak prescribed PF in response to the 45° toe wedge, block under MT1 and MT5. Since tibia and fibula motion remained consistent, it is likely the talus itself was more dorsiflexed relative to the tibia and fibula. This increased talar dorsiflexion has also been observed in studies on weightbearing effects on the ankle and hindfoot joints (Conconi et al., 2024a; Yamaguchi et al., 2009). Second, between peak prescribed DF and PF, TT and TaF joints experienced greater IR when a block was placed under MT1 or when the foot was inverted by 10°. Again, since tibia and fibula motion remained consistent, this increased IR likely originated from the talus. These responses highlight the talus's ability to passively adapt to perturbations in both the sagittal and transverse planes relative to the tibia and fibula during sagittal tibial movement.

In contrast, the hindfoot joints showed significant passive adaptive motions, particularly in the transverse and coronal planes, in response to the perturbations during prescribed tibial DF/PF. When the MTP joint was dorsiflexed with a 45° toe wedge, ST, TN, and CC joints exhibited increased INV and IR between peak prescribed DF and PF. Additionally, CC joint demonstrated increased PF during the same transition periods. Our data suggest that the windlass mechanism may influence the hindfoot joints, particularly the ST joint. Hicks proposed that DF of the MTP joint pre-tensions the plantar fascia, pulling on the calcaneus, shortening and raising the arch, and inverting the ST joint (Bogla and Malone, 2004; Hicks, 1954). Although we cannot directly observe the arch or measure changes in the plantar fascia with MTP joint DF, the increased INV of the ST joint supports an aspect of Hicks's windlass mechanism (Hicks, 1954). Furthermore, MTP joint DF with the 45° toe wedge and resulting ST joint INV may affect the TN and CC joints (i.e., midtarsal joints). We observed kinematic shifts in the all 3 planes of motion in these joints, challenging Elftman's midtarsal locking theory and recent work reporting minimal midtarsal movement during gait (Bruening et al., 2018; Elftman, 1960). However, our data cannot confirm midtarsal locking. Instead, our findings may support a new perspective that the plantar fascia plays a greater role in producing movement during gait via the windlass mechanism (Welte et al., 2021; Welte et al., 2018). In general, the windlass mechanism and midtarsal locking theories pertain to gait. Since our study prescribed planar tibial motions rather than reproduce gait with muscle actuation, our findings offer partial insights into these theories, specifically regarding how plantar fascia pre-tensioning and intrinsic muscles influence hindfoot and midtarsal joint kinematics.

The hindfoot joint passively adapted predictably when comparing the kinematic changes between a block under MT1 and 10° INV versus a block under MT5 and 10° EV. As anticipated, these pairs of perturbations led to contrasting kinematic responses, where a block under MT1 and 10° INV induced increased PF, INV, and IR in the hindfoot joints, while a block under MT5 and 10° EV caused increased DF, EV, and ER. Similar results were observed by Conconi et al., who reported significant movability and displacement in the TN and CC joints with prescribed DF/PF and pronation/supination in weightbearing conditions (Conconi et al., 2024a).

During prescribed tibial ER/IR, TT and TaF joints passively adapted in the sagittal plane predominately. Notably, TaF joint showed decreased ROM with a block under MT1 and 10° INV. Foot INV, even with just a block under MT1 inverting the forefoot and prescribed tibial ER/IR, may limit sagittal TaF joint motion, possibly due to ligamentous constraints. In particular, the posterior and anterior talofibular ligaments (PTFL and ATFL, respectively) may become tensioned and more superiorly oriented with respect to the talus when the foot is inverted, constraining the talus and limiting TaF joint ROM in the sagittal plane during prescribed tibial ER/IR motion. While not directly correlated, previous *in vitro* studies have indicated that the ATFL resists talar ROM,

like anterior translation, inversion, or internal rotation (De Asla et al., 2009; Hubbard, 2008; Rosenbaum et al., 1998). ST, TN, and CC joints passively adapted in the transverse and coronal planes predominantly during prescribed tibial ER/IR, while CC joint showed passive adaptation in the sagittal plane. These passive adaptive responses further highlight the ability of the hindfoot joints to accommodate perturbations, as already demonstrated during prescribed tibial DF/PF.

During prescribed tibial VR/VG, passive adaptive motions were observed in the TT and TaF joints with minimal passive adaptive motions in the ST, TN, and CC joint, primarily at the beginning and/or end of prescribed tibial VR/VG. Compared to the significant amount of passive adaptations in the sagittal and transverse planes, the hindfoot joints appear to have a lesser role in foot mobility during prescribed tibial motion in the coronal plane. This suggests that the hindfoot joints may play a more specialized role in supporting foot mobility and stability during tibial VR/VG, potentially protecting against injuries, such as lateral ankle sprains, caused by abnormal or extreme coronal plane movements at the foot and ankle.

Despite the observed passive adaptive motions throughout the foot and ankle, passive ROM in the examined joints remained consistent across different perturbations. This highlights the interplay between mobility and stability of the joints, suggesting that the ankle and hindfoot can preserve overall mobility, but at the same time, shift the kinematic operating range of individual joints to maintain stability depending on the perturbation. If significant differences were observed in the overall passive ROM, it could indicate injury. To our knowledge, this study is the first to demonstrate this passive adaptability of the ankle and hindfoot.

This study is not without limitations. We studied the passive ankle and hindfoot joint kinematics in a limited sample size with all male specimens. However, our findings align with aspects of previous studies, supporting their general validity (Dubbeldam et al., 2010; Kerrigan et al., 1998). Moreover, MDD for passive joint ROM was approximately 0.1° to 4.0° across all joints, varying slightly by motion plane and prescribed tibial motion. These values indicate that, given the sample size, the study could reliably detect changes of 0.1° or greater in joints with smaller ROM and 4.0° or greater in joints with larger ROM. This limited number of specimens was determined by constraints in the tissue procurement process and the demands on our extensive testing protocol. Furthermore, the use of cadaveric specimens may not fully replicate *in vivo* conditions. However, quantifying the passive kinematics and ROM in the absence of muscle activation is still clinically significant, whereas these baseline measurements produce a fundamental understanding of the foot and ankle's passive mechanical properties. From this baseline, we can better understand how the structures behave once muscle loads and other dynamic forces are applied. Importantly, while tibial rotations were prescribed, off-axis loads were not measured or controlled during the tibial motion profile tuning procedure (Appendix A of the Supplementary Material). These off-axis loads were not the focus of the tuning procedure, which aimed to identify specimen-specific tibial ROM based on shear force or moment thresholds relevant to the prescribed tibial rotation. However, to ensure consistent initial loading across specimens, we applied $25 \pm 2.5\% \text{ BW}$ in the Z-axis (superior-to-inferior direction) in a neutral position prior to each tibial rotation. We acknowledge that unmeasured variation in off-axis loads during tibial rotations may have occurred and represents an area of improvement for future work. Lastly, while we examined the kinematic stability of the joints, we did not directly assess the role of the ligaments. Nevertheless, our study focuses on how passive adaptability illustrates morphology-driven functionality, while inferring some insights into the interaction between the ligaments and joint morphology. Future work will aim to include additional specimens and expand our analysis to investigating the effects of surgical intervention and/or pathologies on the passive ankle and hindfoot joint motions.

5. Conclusion

The data presented in this study highlights the passive adaptability of the individual ankle and hindfoot joints, demonstrating how they adjust to underfoot perturbations through kinematic shifts, in their motions during prescribed planar tibial motion, while maintaining their overall ROM. Our findings emphasize the critical role the talus plays in these adaptations, particularly in the sagittal and transverse planes. This study continues to challenge the traditional view of the TT joint as the primary contributor to foot and ankle mobility, supporting the notion that other joints play more dynamic roles during lower limb ground interactions. Notably, the ST, TN, and CC joints demonstrated significant passive adaptive responses to perturbations in the transverse and coronal planes, underscoring their importance in both stability and mobility. By examining the individual passive joint kinematics, we can gain crucial insights into the underlying mechanics that contribute to overall foot and ankle mobility and stability. Future research should investigate the impact of pathologies and surgical interventions on these passive adaptations.

CRediT authorship contribution statement

Anthony H. Le: Writing – review & editing, Writing – original draft, Visualization, Validation, Software, Methodology, Investigation, Formal analysis, Data curation, Conceptualization. **Andrew C. Peterson:** Writing – review & editing, Validation, Software. **Jordy A. Larrea Rodríguez:** Writing – review & editing, Validation, Software. **Takuma Miyamoto:** Writing – review & editing. **Florian Nickisch:** Writing – review & editing, Supervision. **Amy L. Lenz:** Writing – review & editing, Supervision, Project administration, Methodology, Investigation, Funding acquisition, Conceptualization.

Declaration of competing interest

The authors declare that they have no known competing financial interests or personal relationships that could have appeared to influence the work reported in this paper.

Acknowledgments

We would like to thank Paragon 28, Inc. and Richard Obert from FOCUS Medical Design & Development via Paragon 28, Inc. for their additional technical support in experimental setup and testing. This work was financially supported by a research contract with Paragon 28, Inc.

Appendix A. Supplementary data

Supplementary data to this article can be found online at <https://doi.org/10.1016/j.biomech.2025.112740>.

Data availability

Data will be made available on request.

References

- Arndt, A., Wolf, P., Liu, A., Nester, C., Stacoff, A., Jones, R., Lundgren, P., Lundberg, A., 2007. Intrinsic foot kinematics measured in vivo during the stance phase of slow running. *J. Biomech.* 40, 2672–2678.
- Aubin, P., Ledoux, W.R., 2023. Chapter 22 - Cadaveric Gait Simulation. In: Ledoux, W.R., Telfer, S. (Eds.), *Foot and Ankle Biomechanics*. Academic Press, pp. 351–363.
- Aubin, P.M., Cowley, M.S., Ledoux, W.R., 2008. Gait Simulation via a 6-DOF Parallel Robot With Iterative Learning Control. *IEEE Trans. Biomed. Eng.* 55, 1237–1240.
- Aubin, P.M., Whittaker, E., Ledoux, W.R., 2011. A robotic cadaveric gait simulator with fuzzy logic vertical ground reaction force control. *IEEE Trans. Rob.* 28, 246–255.
- Baxter, J.R., Sturnick, D.R., Demetracopoulos, C.A., Ellis, S.J., Deland, J.T., 2016. Cadaveric gait simulation reproduces foot and ankle kinematics from population-specific inputs. *J. Orthop. Res.* 34, 1663–1668.
- Bey, M.J., Kline, S.K., Tashman, S., Zauel, R., 2008. Accuracy of biplane x-ray imaging combined with model-based tracking for measuring in-vivo patellofemoral joint motion. *J. Orthop. Surg. Res.* 3, 1–8.
- Bey, M.J., Zauel, R., Brock, S.K., Tashman, S., 2006. Validation of a new model-based tracking technique for measuring three-dimensional, in vivo glenohumeral joint kinematics.
- Bolgla, L.A., Malone, T.R., 2004. Plantar fasciitis and the windlass mechanism: a biomechanical link to clinical practice. *J. Athl. Train.* 39, 77.
- Bruenig, D.A., Pohl, M.B., Takahashi, K.Z., Barrios, J.A., 2018. Midtarsal locking, the windlass mechanism, and running strike pattern: a kinematic and kinetic assessment. *J. Biomech.* 73, 185–191.
- Burssens, A., Krähenbühl, N., Lenz, A.L., Howell, K., Zhang, C., Sripanich, Y., Saltzman, C.L., Barg, A., 2021. Interaction of loading and ligament injuries in subtalar joint instability quantified by 3D weightbearing computed tomography. *Journal of Orthopaedic Research®*.
- Campbell, K.J., Wilson, K.J., LaPrade, R.F., Clanton, T.O., 2016. Normative rearfoot motion during barefoot and shod walking using biplane fluoroscopy. *Knee Surg. Sports Traumatol. Arthrosc.* 24, 1402–1408.
- Conconi, M., Pompili, A., Sancisi, N., Durante, S., Leardini, A., Belvedere, C., 2024a. Foot kinematics as a function of ground orientation and weightbearing. *Journal of Orthopaedic Research®* 42, 148–163.
- Conconi, M., Sancisi, N., Leardini, A., Belvedere, C., 2024b. The foot and ankle complex as a four degrees-of-freedom system: Kinematic coupling among the foot bones. *Journal of Orthopaedic Research®*.
- De Asla, R.J., Kozánek, M., Wan, L., Rubash, H.E., Li, G., 2009. Function of anterior talofibular and calcaneofibular ligaments during in-vivo motion of the ankle joint complex. *J. Orthop. Surg. Res.* 4, 1–6.
- Downey, R.J., Richer, N., Gupta, R., Liu, C., Pliner, E.M., Roy, A., Hwang, J., Clark, D.J., Hass, C.J., Manini, T.M., 2022. Uneven terrain treadmill walking in younger and older adults. *PLoS One* 17, e0278646.
- Dubbeldam, R., Buirke, J., Simons, C., Grootenhuis-Oudshoorn, C., Baan, H., Nene, A., Hermens, H., 2010. The effects of walking speed on forefoot, hindfoot and ankle joint motion. *Clin. Biomech.* 25, 796–801.
- Elftman, H., 1960. The transverse tarsal joint and its control. *Clinical Orthopaedics and Related Research®* 16, 41–46.
- Grood, E.S., Suntay, W.J., 1983. A joint coordinate system for the clinical description of three-dimensional motions: application to the knee. *J. Biomech. Eng.* 105, 136–144.
- Hicks, J., 1954. The mechanics of the foot: II. The plantar aponeurosis and the arch. *J. Anat.* 88, 25.
- Hubbard, T.J., 2008. Ligament laxity following inversion injury with and without chronic ankle instability. *Foot Ankle Int.* 29, 305–311.
- Kapron, A.L., Aoki, S.K., Peters, C.L., Maas, S.A., Bey, M.J., Zauel, R., Anderson, A.E., 2014. Accuracy and feasibility of dual fluoroscopy and model-based tracking to quantify in vivo hip kinematics during clinical exams. *J. Appl. Biomech.* 30, 461–470.
- Kerrigan, D.C., Todd, M.K., Della Croce, U., Lipsitz, L.A., Collins, J.J., 1998. Biomechanical gait alterations independent of speed in the healthy elderly: evidence for specific limiting impairments. *Arch. Phys. Med. Rehabil.* 79, 317–322.
- Knutson, K., Muhlrad, E.P., Peterson, A.C., Leonard, T., Anderson, A.M., Aragon, K.C., Eatough, Z.J., MacWilliams, B.A., Kruger, K.M., Lenz, A.L., 2024. Talar and calcaneal coordinate axes definitions across foot pathologies. *J. Biomech.* 175, 112298.
- Lenz, A., Strobel, M.A., Anderson, A.M., Fial, A.V., MacWilliams, B.A., Krzak, J.J., Kruger, K.M., 2021. Assignment of local coordinate systems and methods to calculate tibiotalar and subtalar kinematics: A systematic review. *J. Biomech.* 110344.
- Lundgren, P., Nester, C., Liu, A., Arndt, A., Jones, R., Stacoff, A., Wolf, P., Lundberg, A., 2008. Invasive in vivo measurement of rear-, mid-and forefoot motion during walking. *Gait Posture* 28, 93–100.
- MacWilliams, B.A., Davis, R.B., 2013. Addressing Some Misperceptions of the Joint Coordinate System. *J. Biomech. Eng.* 135, 54506.
- Miyamoto, T., Otake, Y., Nakao, S., Kurokawa, H., Kosugi, S., Taniguchi, A., Soufi, M., Sato, Y., Tanaka, Y., 2023. 4D-foot analysis on effect of arch support on ankle, subtalar, and talonavicular joint kinematics. *J. Orthop. Sci.*
- Muhlrad, E.P., Peterson, A.C., Anderson, A.M., Aragon, K.C., Lisonbee, R.J., MacWilliams, B.A., Kruger, K.M., Lenz, A.L., 2024. Recommendation of minimal distal tibial length for long axis coordinate system definitions. *J. Biomech.* 170, 112153.
- Nester, C., Liu, A., Ward, E., Howard, D., Cocheba, J., Derrick, T., Patterson, P., 2007. In vitro study of foot kinematics using a dynamic walking cadaver model. *J. Biomech.* 40, 1927–1937.
- Nichols, T.E., Holmes, A.P., 2002. Nonparametric permutation tests for functional neuroimaging: a primer with examples. *Hum. Brain Mapp.* 15, 1–25.
- Noble, L.D., Colbrunn, R.W., Lee, D.-G., Van Den Bogert, A.J., Davis, B.L., 2010. Design and Validation of a General Purpose Robotic Testing System for Musculoskeletal Applications. *J. Biomech. Eng.* 132, 025001.
- Pataky, T.C., 2010. Generalized n-dimensional biomechanical field analysis using statistical parametric mapping. *J. Biomech.* 43, 1976–1982.
- Pataky, T.C., Robinson, M.A., Vanrenterghem, J., 2013. Vector field statistical analysis of kinematic and force trajectories. *J. Biomech.* 46, 2394–2401.
- Pataky, T.C., Robinson, M.A., Vanrenterghem, J., 2016. Region-of-interest analyses of one-dimensional biomechanical trajectories: bridging 0D and 1D theory, augmenting statistical power. *PeerJ* 4, e2652.
- Pataky, T.C., Vanrenterghem, J., Robinson, M.A., 2015. Zero-vs. one-dimensional, parametric vs. non-parametric, and confidence interval vs. hypothesis testing

- procedures in one-dimensional biomechanical trajectory analysis. *J. Biomech.* 48, 1277–1285.
- Peterson, A.C., Kruger, K.M., Lenz, A.L., 2023. Automatic anatomical foot and ankle coordinate toolbox. *Front. Bioeng. Biotechnol.* 11.
- Postolka, B., Killen, B.A., Boey, H., Malaquias, T.M., Natsakis, T., Clockaerts, S., Misselyn, D., Coudyzer, W., Vander Sloten, J., Jonkers, I., 2024. Hindfoot kinematics and kinetics-A combined in vivo and in silico analysis approach. *Gait Posture* 112, 8–15.
- Roach, K.E., Wang, B., Kapron, A.L., Fiorentino, N.M., Saltzman, C.L., Bo Foreman, K., Anderson, A.E., 2016. In Vivo Kinematics of the Tibiotalar and Subtalar Joints in Asymptomatic Subjects: A High-Speed Dual Fluoroscopy Study. *J. Biomed. Eng.* 138, 091006.
- Rosenbaum, D., Becker, H., Wilke, H.-J., Claes, L., 1998. Tenodeses destroy the kinematic coupling of the ankle joint complex: a three-dimensional in vitro analysis of joint movement. *J. Bone Joint Surg. British* 80, 162–168.
- Salb, K.N., Wido, D.M., Stewart, T.E., Diangelo, D.J., 2016. Development of a Robotic Assembly for Analyzing the Instantaneous Axis of Rotation of the Foot Ankle Complex. *Appl. Bionics Biomech.* 2016, 1–9.
- Tuijthof, G.J.M., Zengerink, M., Beimers, L., Jonges, R., Maas, M., van Dijk, C.N., Blankevoort, L., 2009. Determination of consistent patterns of range of motion in the ankle joint with a computed tomography stress-test. *Clin. Biomech.* 24, 517–523.
- Wang, B., Roach, K.E., Kapron, A.L., Fiorentino, N.M., Saltzman, C.L., Singer, M., Anderson, A.E., 2015. Accuracy and feasibility of high-speed dual fluoroscopy and model-based tracking to measure in vivo ankle arthrokinematics. *Gait Posture* 41, 888–893.
- Welte, L., Kelly, L.A., Kessler, S.E., Lieberman, D.E., D'Andrea, S.E., Lichtwark, G.A., Rainbow, M.J., 2021. The extensibility of the plantar fascia influences the windlass mechanism during human running. *Proc. R. Soc. B* 288, 20202095.
- Welte, L., Kelly, L.A., Lichtwark, G.A., Rainbow, M.J., 2018. Influence of the windlass mechanism on arch-spring mechanics during dynamic foot arch deformation. *J. R. Soc. Interface* 15, 20180270.
- Whittaker, E.C., Aubin, P.M., Ledoux, W.R., 2011. Foot bone kinematics as measured in a cadaveric robotic gait simulator. *Gait Posture* 33, 645–650.
- Wu, G., van der Helm, F.C.T., Veeger, H.E.J., Makhsoos, M., Van Roy, P., Anglin, C., Nagels, J., Karduna, A.R., McQuade, K., Wang, X., Werner, F.W., Buchholz, B., 2005. ISB recommendation on definitions of joint coordinate systems of various joints for the reporting of human joint motion—Part II: shoulder, elbow, wrist and hand. *J. Biomed.* 38, 981–992.
- Yamaguchi, S., Sasho, T., Kato, H., Kuroyanagi, Y., Banks, S.A., 2009. Ankle and subtalar kinematics during dorsiflexion-plantarflexion activities. *Foot Ankle Int.* 30, 361–366.